Monthly Notices
of the
ROYAL ASTRONOMICAL SOCIETY

Mon. Not. R. Astron. Soc. **420,** 3035–3046 (2012) doi:10.1111/j.1365-2966.2011.20177.x

Magnetar oscillations – II. Spectral method

Maarten van Hoven[1,2⋆] and Yuri Levin[1,2,3]

[1]*Leiden Observatory, Leiden University, PO Box 9513, NL-2300 RA Leiden, the Netherlands*
[2]*Lorentz Institute, Leiden University, Niels Bohrweg 2, NL-2333 CA Leiden, the Netherlands*
[3]*School of Physics, Monash University, PO Box 27, VIC 3800, Australia*

Accepted 2011 November 9. Received 2011 November 4; in original form 2011 October 10

ABSTRACT

The seismological dynamics of magnetars are largely determined by a strong hydromagnetic coupling between the solid crust and the fluid core. In this paper, we set up a 'spectral' computational framework in which the magnetar's motion is decomposed into a series of basis functions that are associated with the crust and core vibrational eigenmodes. A general relativistic formalism is presented for evaluation of the core Alfvén modes in the magnetic flux coordinates, as well for eigenmode computation of a strongly magnetized crust of finite thickness. By considering coupling of the crustal modes to the continuum of Alfvén modes in the core, we construct a fully relativistic dynamical model of the magnetar which allows: (i) fast and long simulations without numerical dissipation; and (ii) very fine sampling of the stellar structure. We find that the presence of strong magnetic field in the crust results in localizing of some high-frequency crustal elastomagnetic modes with the radial number $n \geq 1$ to the regions of the crust where the field is nearly horizontal. While the hydromagnetic coupling of these localized modes to the Alfvén continuum in the core is reduced, their energy is drained on a time-scale of $\ll 1$ s. Therefore, the puzzle of quasi-periodic oscillations with frequencies larger than 600 Hz still stands.

Key words: stars: neutron.

1 INTRODUCTION

Magnetar oscillations have been subject of extensive theoretical research since the discovery of quasi-periodic oscillations (QPOs) in the light curves of giant flares from soft gamma repeaters (SGRs) (Israel et al. 2005; Strohmayer & Watts 2005; Watts & Strohmayer 2006; see also Barat et al. 1983). The observed oscillations are measured with high signal-to-noise ratios during time-intervals of typically few minutes in the frequency range 18–1800 Hz. It has been proposed by many authors that the physical origin of the QPOs is seismic vibrations of the star; an idea which opens the possibility to perform asteroseismological analysis of neutron stars, giving a unique observational window into the stellar interior. Initially it was hypothesized that the observed oscillations originate from torsional shear modes which are confined to the magnetar crust (e.g. Duncan 1998; Piro 2005; Watts & Strohmayer 2006; Samuelsson & Andersson 2007, hereafter SA; Watts & Reddy 2007; Steiner & Watts 2009). If this hypothesis were true, then the observed QPOs would strongly constrain physical parameters in the neutron star crust. However, it was soon realized that, due to the presence of ultrastrong magnetic fields ($B \sim 10^{14}$–10^{15} G; Kouveliotou et al. 1999) which are frozen both in the crust and in the core of the star, the crustal motion is strongly coupled to the fluid core on time-scales $\ll 1$ s (Levin 2006, hereafter L06). Over the years, several authors have studied the coupled crust–core problem (Glampedakis, Samuelsson & Andersson 2006; Levin 2007, hereafter L07; Gruzinov 2008; Lee 2008; Colaiuda & Kokkotas 2011; Gabler et al. 2011a,b; van Hoven & Levin 2011, hereafter Paper I). In particular, L06 and L07 argued that for sufficiently simple magnetic field configurations (i.e. axisymmetric poloidal fields), the Alfvén-type motions on different flux surfaces are decoupled so that the Alfvén frequencies in the core feature a continuum. This result is well known from previous magnetohydrodynamic (MHD) studies, and it applies to general axisymmetric poloidal–toroidal magnetic fields (Poedts, Hermans & Goossens 1985). It allows one to describe the problem of magnetar dynamics in terms of discrete crustal modes that couple to a continuum of Alfvén modes in the core. With this approach, L07 and Paper I demonstrated that the presence of an Alfvén continuum has some important implications for magnetar oscillations: (i) global modes of the star with frequencies that are located inside the continuum undergo strong exponential damping [this phenomenon is often called *resonant absorption* in the context of MHD (Goedbloed & Poedts 2004)]; and (ii) after the initial period (<1 s) of exponential decay, the system tends to settle in a steady state in which it oscillates at frequencies close to the edges of the continuum; these oscillations correspond to the so-called *edge modes*, which were first seen numerically in L07 and Gruzinov

⋆E-mail: vhoven@strw.leidenuniv.nl (MvH); yuri@strw.leidenuniv.nl (YL)

(2008), and were explained analytically in Paper I. The edge modes were further observed in the simulations of Gabler et al. (2011a,b) and Colaiuda & Kokkotas (2011).

In the past half-decade, two distinct computational strategies have been applied to the problem of calculating magnetar oscillations:

(1) Several groups employed general relativistic MHD grid codes to simulate the dynamics of magnetized neutron stars. Sotani, Kokkotas & Stergioulas (2008), Colaiuda, Beyer & Kokkotas (2009) and Cerdá-Durán, Stergioulas & Font (2009) were able to reproduce continuum Alfvén modes in the purely fluid stars with axisymmetric poloidal magnetic field, which provided important benchmark tests for the ability of the codes to handle complex MHD oscillations. Building on this, Gabler et al. (2011a,b) and Colaiuda & Kokkotas (2011) included a crust in their neutron star models, and were thus able to study the coupled dynamics of the crust and the core.

(2) Our group (L07 and Paper I) and Lee (2008) decomposed the motion of a magnetar into a set of basis functions, and studied the dynamics of the coefficients of these series expansions; we shall refer to this strategy as the 'spectral method'. This framework is able to handle both the dynamical simulations and the stationary eigenmode problem; the latter reduces to solving the eigenvalue problem for a large matrix. L07 and Paper I chose the basis functions so that the crustal motion is decomposed into the normal modes of the free crust, and the core motion is decomposed into the sum of core Alfvén modes and a separate contribution of the core's 'dc' displacements in reaction to the motion of the crust. We refer the reader to section 3.2 of L07, section 4.2 of Paper I and Section 4.2 of this paper for technical details. This choice of basis functions casts the dynamics of magnetars as a problem of coupled harmonic oscillators, in which the discrete modes of the crust are coupled to the Alfvén modes in the core.

The computations of Paper I have been performed using Newtonian equations of motion and in the limit of a thin crust. In this paper, we improve on Paper I in two ways: (i) we adopt a realistic crust of finite thickness, threaded with a strong magnetic field; and (ii) we employ fully relativistic equations governing the motion of axial perturbations in the crust and the core. Our spectral method has several practical and conceptual advantages: (i) it is numerically inexpensive, making implementation of long simulations of the magnetar dynamics in an ordinary workstation possible; (ii) it allows one to sample the stellar structure at high spatial resolution; (iii) it does not suffer from the problem of numerical viscosity that occurs in some finite difference schemes (scaling with the grid size); and (iv) it is able to handle arbitrary axisymmetric poloidal fields, and not just those that are the solutions of the Grad–Shafranov (GS) equation.[1]

The outline of this paper is as follows. In Section 2, we derive relativistic equations describing the magnetic forces acting on axial perturbations inside a neutron star with an axisymmetric poloidal magnetic field. We construct a coordinate system which has one of its axes parallel to the field lines. The equations thus obtained will be discussed in later sections when we calculate elastomagnetic modes of the crust, and when we calculate the Alfvén continuum in the core.

In Section 3.1, we introduce a formalism which allows us to calculate general relativistic elastomagnetic eigenmodes of the crust by expanding the elastomagnetic equations of motion in a set of basis functions. This reduces the eigenmode problem of the crust to a matrix eigenvalue problem. In Sections 3.2 and 3.3, we work out the relativistic equations describing the magnetic and elastic restoring-force densities in the curved space–time of the neutron star crust. In Section 3.4, we apply these equations to the formalism of Section 3.1 in order to find free crustal eigenmodes and eigenfrequencies.

In Section 4, we find the core continuum Alfvén modes in full general relativity, and we calculate their coupling to the crustal modes of Section 3. The magnetar model constructed in this way qualitatively shows the same features of the Paper I model, that is, above the fundamental Alfvén frequency of ∼20 Hz; the frequency domain is covered by the core continuum which effectively acts to damp crustal motion. For particular choices of the field configuration, the continuum may contain a number of gaps, generally well below 200 Hz. These gaps give rise to the characteristic 'edge modes' of Paper I. Moreover, the crustal modes that reside inside gaps remain undamped. In the appendix, we revisit the problem of crustal mode damping due to the presence of an Alfvén continuum, by analytically calculating damping rates according to Fermi's golden rule.

2 RELATIVISTIC EQUATIONS FOR MAGNETIC FORCES

Magnetic coordinates

We shall consider strongly subequipartition $B \ll 10^{18}$ G magnetic fields, so that the physical deformation of the star is very small and the space–time is spherically symmetric with respect to the star's centre. The metric can be written in the standard Schwarzschild-type coordinates r, θ and ϕ. It is natural, in analogy with the Newtonian treatments, to introduce the flux coordinate system in which one of the axes is parallel to the magnetic field lines (the precise meaning of this construction in relativity is described below). In the axisymmetric poloidal field geometry, the magnetic field lines are located in planes of constant azimuthal angle ϕ, which allows us to define the two 'magnetic' coordinates $\chi(r, \theta)$ and $\psi(r, \theta)$, such that the (covariant) vectors $\boldsymbol{e}_\phi = \partial/\partial\phi$ and $\boldsymbol{e}_\chi = \partial/\partial\chi$ are orthogonal to $\boldsymbol{e}_\psi = \partial/\partial\psi$. In the flux coordinate system, the metric is given by

$$\begin{aligned} \mathrm{d}s^2 = &-g_{tt}\mathrm{d}t^2 + g_{\chi\chi}\mathrm{d}\chi^2 + g_{\psi\psi}\mathrm{d}\psi^2 \\ &+ 2g_{\psi\chi}\mathrm{d}\chi\mathrm{d}\psi + g_{\phi\phi}\mathrm{d}\phi^2, \end{aligned} \tag{1}$$

while the magnetic field vector is given by

$$\boldsymbol{B} = B^\chi \boldsymbol{e}_\chi. \tag{2}$$

Here $\boldsymbol{B}$ is the 4-vector whose components are given by

$$B^\mu = \frac{1}{2}\epsilon^{\mu\nu\alpha\beta}F_{\alpha\beta}v_\nu, \tag{3}$$

where v_ν is the 4-velocity vector which for the stationary star is given by $v_t = g_{tt}v^t = \sqrt{-g_{tt}}$, $v_i = 0$.

Clearly, g_{tt} and $g_{\phi\phi}$ are identical to the corresponding Schwarzschild metric terms,

$$\begin{aligned} g_{tt} &= 1 - \frac{2m(r)}{r}, \\ g_{\phi\phi} &= r^2\sin^2\theta\,. \end{aligned} \tag{4}$$

[1] The approach developed by Sotani et al. (2008) and used in Colaiuda et al. (2009) and Colaiuda & Kokkotas (2011) casts the MHD equations in the core into a particularly simple form. This transformation is possible if the poloidal field is the solution of the GS equation. There is, however, no compelling reason why the GS equation should hold, since neutron stars feature very strong stable stratification due to the radial gradients in proton-to-neutron ratios (Goldreich & Reisenegger 1992; Mastrano et al. 2011).

Maxwell's equations

The evolution of the magnetic field is described by Maxwell's equations. In curved space–time, these read

$$F_{\mu\nu;\lambda} + F_{\lambda\mu;\nu} + F_{\nu\lambda;\mu} = 0. \tag{5}$$

In the ideal MHD limit, the electric field $E_\mu = v^\nu F_{\mu\nu}$ vanishes so that the only contribution to the electromagnetic tensor comes from the magnetic field:

$$F_{\mu\nu} = -\epsilon_{\mu\nu\lambda\sigma} v^\lambda B^\sigma. \tag{6}$$

After some manipulation, relations (5) and (6) yield the MHD equation for the magnetic field:

$$(v^\mu B^\nu - v^\nu B^\mu)_{;\mu} = 0. \tag{7}$$

This equation entails both magnetic induction, which describes the flux freezing that characterizes magnetic fields in the ideal MHD approximation, and Gauss' law for magnetic fields, that is, $(v^\mu B^t - v^t B^\mu)_{;\mu} = 0$. For a static equilibrium, that is, $v_t = \sqrt{-g_{tt}}$ and $v_i = 0$ (where the index i runs over the spatial indices), Gauss' law can be expressed in the more familiar form

$$B^i_{;i} = \frac{1}{\sqrt{g}} \left(\sqrt{g} B^i\right)_{,i} = 0, \tag{8}$$

where $g \equiv \det(g_{ij})/g_{tt}$. This expression provides the basis for a convenient map between magnetic fields of Newtonian and relativistic stars. In the Newtonian case, the flux coordinates χ and ψ are functions of r and θ; we keep this functional form for the relativistic versions of χ and ψ. The expression in equation (8) is valid both in the curved space–time and in the flat Euclidean space (with g_{ij} is replaced by the Euclidean metric terms) of the Newtonian star. We can therefore use equation (8) to convert the values of the Euclidean field, $B_{\rm E}$, to the correct values of the magnetic field in curved space–time, $B_{\rm S}$ (the subscript E stands again for *Euclidean* and S for *Schwarzschild*): equation (8) gives $\left(\sqrt{g_{\rm S}} B^i_{\rm S}\right)_{,i} = \left(\sqrt{g_{\rm E}} B^i_{\rm E}\right)_{,i} = 0$. We thus obtain

$$B^\chi_{\rm S} = \frac{\sqrt{g_{\rm E}}}{\sqrt{g_{\rm S}}} B^\chi_{\rm E} = \frac{1}{\sqrt{g_{rr}}} B^\chi_{\rm E}, \tag{9}$$

which results in the relativistic poloidal magnetic field which is tangent to the flux surfaces $\psi =$ constant and which satisfies Gauss' law. (In the following, we will drop the subscript S.) In this work, for concreteness, we use the Newtonian configuration of the magnetic field generated by a current loop inside the neutron star and discussed in detail in Paper I. Other Newtonian configurations are readily mapped on to the relativistic configurations using the procedure specified above.

Euler equations

The equations of motion are obtained by enforcing conservation of momentum, that is, by projecting the conservation of energy momentum 4-vector on the space normal to the 4-velocity v^λ:

$$h^\lambda_\mu T^{\mu\nu}_{;\nu} = 0, \tag{10}$$

where the projection tensor h^λ_μ is given by

$$h^\lambda_\mu = \delta^\lambda_\mu + v^\lambda v_\mu. \tag{11}$$

$T^{\mu\nu}$ is the stress energy tensor for a magnetized fluid in the ideal MHD approximation and can be expressed as

$$T^{\mu\nu} = \left(\rho + P + \frac{B^2}{4\pi}\right) v^\mu v^\nu + \left(P + \frac{B^2}{8\pi}\right) g^{\mu\nu} - \frac{B^\mu B^\nu}{4\pi}, \tag{12}$$

where ρ and P are the mass density and pressure and $B^2 = B^\mu B_\mu$ is the square of the magnetic field, where $B_\mu = \frac{1}{2}\epsilon_{\mu\nu\lambda\sigma} u^\nu F^{\lambda\sigma}$ is the covariant component of the Lorentz invariant magnetic field 4-vector ($\epsilon_{\mu\nu\lambda\sigma}$ is the four-dimensional Levi–Civita symbol and $F^{\lambda\sigma}$ is the electromagnetic tensor). The equations of motion become

$$\left(\rho + P + \frac{B^2}{4\pi}\right) v^\mu_{;\nu} v^\nu = h^{\mu\lambda} \left(P + \frac{B^2}{8\pi}\right)_{;\lambda} + h^\mu_\sigma \left(\frac{B^\sigma B^\lambda}{4\pi}\right)_{;\lambda}. \tag{13}$$

Here we have used the relation $v_\nu v^\nu = g_{\mu\nu} v^\mu v^\nu = -1$. Equation (13) together with equation (7) provides a full description of (incompressible) motion of the magnetized fluid in a neutron star.

Perturbation equations

We are now ready to derive equations that describe the linearized motion of a small Lagrangian fluid displacement ζ^μ about the static background equilibrium of the star. The perturbed components of the velocity and the magnetic field 4-vectors, $v^\mu_{\rm pert}$ and $B^\mu_{\rm pert}$, are

$$\begin{aligned} v^\mu_{\rm pert} &= v^\mu + \delta v^\mu = v^\mu + \frac{\partial \zeta^\mu}{\partial \tau}, \\ B^\mu_{\rm pert} &= B^\mu + \delta B^\mu, \end{aligned} \tag{14}$$

where the first terms on the right-hand side denote the unperturbed equilibrium quantities, and the second terms on the right-hand side denote the Eulerian perturbations associated with the displacement ζ^μ. In our 'magnetic' coordinates, the only non-zero component of the unperturbed magnetic field is $B^\chi = B/\sqrt{g_{\chi\chi}}$, and because the equilibrium star is static and non-rotating the only non-zero component of the 4-velocity is $v^t = 1/\sqrt{-g_{tt}}$. Restricting ourselves to axisymmetric torsional oscillations of the star, we introduce a small incompressible axisymmetric displacement ζ^ϕ. This implies that $v^\mu_{{\rm pert};\mu} = \delta v^\mu_{;\mu} = \delta v^t_{;t}$, and that the perturbations in pressure, δP, and mass density, $\delta\rho$, vanish. Technically, a full description of the linearized motion of a neutron star would involve perturbations of the metric $g_{\mu\nu}$, requiring one to augment the above equations of motion with the perturbed Einstein equations. However, since we are considering incompressional axial oscillations only, the metric perturbations are dominated by the current dipole moment. One can show that this causes perturbations in the off-diagonal elements of the metric tensor which are of the order of δv^2, so that the metric perturbations can be safely ignored (the so-called Cowling approximation). Taking these considerations into account, we linearize equations (13) and (7) and after some work we obtain

$$\left(\rho + P + \frac{B^2}{4\pi}\right) \frac{\partial^2 \zeta^\phi}{\partial t^2} = \sqrt{\frac{g_{tt}}{g_{\chi\chi}}} \frac{B}{4\pi g_{\phi\phi}} \frac{\partial}{\partial \chi} \left(g_{\phi\phi} \sqrt{-g_{tt}} \delta B^\phi\right) \tag{15}$$

and

$$\delta B^\phi = \frac{B}{\sqrt{g_{\chi\chi}}} \frac{\partial \zeta^\phi}{\partial \chi}. \tag{16}$$

These equations can be combined into a single equation. After restoring a factor of c^2, we find

$$\left(\rho + \frac{P}{c^2} + \frac{B^2}{4\pi c^2}\right) \frac{\partial^2 \xi}{\partial t^2} = \sqrt{\frac{g_{tt}}{g_{\chi\chi}}} \frac{B}{4\pi c^2 \sqrt{g_{\phi\phi}}} \frac{\partial}{\partial \chi} \left[\sqrt{\frac{g_{tt}}{g_{\chi\chi}}} g_{\phi\phi} B \frac{\partial}{\partial \chi} \left(\frac{\xi}{\sqrt{g_{\phi\phi}}}\right)\right], \tag{17}$$

where $\xi = \sqrt{g_{\phi\phi}} \zeta^\phi$ is the physical displacement (in the ϕ direction) in unit length. This equation describes Alfvén waves travelling along magnetic field lines in the curved space–time of a magnetar. We checked that in the non-relativistic limit equation (17) reduces to the correct expression for Alfvén waves in self-gravitating magnetostatic equilibria (Poedts et al. 1985).

3 MODES OF A MAGNETIZED CRUST IN GENERAL RELATIVITY

In this section, we will describe a formalism that allows us to calculate relativistic eigenmodes and eigenfrequencies of a neutron star crust of finite thickness and realistic equation of state, threaded with an arbitrary magnetic field. By considering a crust of finite thickness, we will obtain high-frequency radial harmonics that are not present in the crust model of Paper I but which should be taken into account in view of the observed high-frequency QPOs. In the past, several authors carried out theoretical analyses of torsional oscillations of neutron stars with a magnetized crust. Carroll et al. (1986), Piro (2005), Glampedakis et al. (2006) and Steiner & Watts (2009) considered horizontal shear waves in a plane-parallel crust threaded by a vertical magnetic field, whereas Sotani, Kokkotas & Stergioulas (2007) have performed the first study of magnetized crusts in general relativity. These authors wrote down equations of motion for the crust with the frozen-in dipole field but then simplified their system of equations by neglecting $l \rightarrow l \pm 2$ couplings. Effectively, this procedure substitutes the dipole field with an l-dependent split-monopole field, enforcing the spherical symmetry for the elastic-MHD equations and restricting the eigenfunctions to be vector spherical harmonics. Lee (2008), on the other hand, studied the Newtonian dynamics of spherical neutron stars with a dipole field, by decomposing the perturbed quantities into a set of basis functions, and following the dynamics of the expansion coefficients. Here we follow a strategy which is closely related to that of Lee (2008), but generalize his treatment to general relativity and arbitrary axisymmetric poloidal fields and find normal modes of the magnetized neutron star crust in the absence of external forces. The hydromagnetic coupling of the crust normal modes obtained in this section, to the core Alfvén modes, will be discussed further in Section 4.

Formalism for finding crustal eigenmodes

In a magnetized and elastic crust, the motion of a small torsional Lagrangian displacement away from equilibrium $\bar{\boldsymbol{\xi}}(\boldsymbol{x}, t)$ (we use the notation from Paper I; $\bar{\xi}$ denotes crustal displacements, ξ denotes displacements in the core) can be described in the general form

$$\frac{\partial^2 \bar{\boldsymbol{\xi}}}{\partial t^2} = \boldsymbol{L}_{\rm el}(\bar{\boldsymbol{\xi}}) + \boldsymbol{L}_{\rm mag}(\bar{\boldsymbol{\xi}}), \tag{18}$$

where $\boldsymbol{L}_{\rm el}$ and $\boldsymbol{L}_{\rm mag}$ are the accelerations due to the elastic and magnetic forces acting on the displacement field. Expressions for $\boldsymbol{L}_{\rm el}$ and $\boldsymbol{L}_{\rm mag}$ are given and discussed in the next subsection. Augmented with no-tangential-stress conditions, $\delta T_{r\phi} = \delta T_{r\theta} = 0$, on the inner and outer boundaries, this equation describes the free oscillations of a magnetized neutron star crust. Our procedure for solving equation (18) is as follows:

First, we decompose the crustal displacement field $\bar{\boldsymbol{\xi}}(t, \boldsymbol{x})$ into a set of basis functions $\boldsymbol{\Psi}_i(\boldsymbol{x})$,

$$\bar{\boldsymbol{\xi}}(t, \boldsymbol{x}) = \sum_{i=1}^{\infty} a_i(t) \boldsymbol{\Psi}_i(\boldsymbol{x}). \tag{19}$$

The functions $\boldsymbol{\Psi}_i$ form an orthonormal basis for a Hilbert space with the inner product

$$\langle \boldsymbol{\eta} | \boldsymbol{\zeta} \rangle = \int_{\mathcal{V}} w(\boldsymbol{x}) \boldsymbol{\eta} \cdot \boldsymbol{\zeta} \, {\rm d}^3 x, \tag{20}$$

where $\boldsymbol{\eta}$ and $\boldsymbol{\zeta}$ are arbitrary functions defined in the volume $\mathcal{V}$ of the crust, and $w(\boldsymbol{x})$ is a weight function. Orthonormality of $\boldsymbol{\Psi}_i(\boldsymbol{x})$ implies that $\langle \boldsymbol{\Psi}_i | \boldsymbol{\Psi}_j \rangle = \delta_{ij}$, where δ_{ij} is the Kronecker delta. The coefficients a_i of the expansion of equation (19) are then simply $a_i(t) = \langle \bar{\boldsymbol{\xi}}(t, \boldsymbol{x}) | \boldsymbol{\Psi}_i(\boldsymbol{x}) \rangle$.

Secondly, we decompose the acceleration field of equation (18) into basis functions $\boldsymbol{\Psi}_i$ according to equation (19), and to calculate the matrix elements $\langle \partial^2 \bar{\boldsymbol{\xi}} / \partial t^2 | \Psi_j \rangle$. This yields equations of motion for $a_i(t)$:

$$\ddot{a}_j = M_{ij} a_i, \tag{21}$$

where the double dot denotes double differentiation with respect to time, and

$$M_{ij} = \left(\langle \boldsymbol{L}_{\rm el}(\boldsymbol{\Psi}_i) | \boldsymbol{\Psi}_j \rangle + \langle \boldsymbol{L}_{\rm mag}(\boldsymbol{\Psi}_i) | \boldsymbol{\Psi}_j \rangle \right),$$

Clearly, a crustal eigenmode with frequency ω_m (i.e. $a_{m,i} \propto {\rm e}^{{\rm i}\omega_m t}$ for all i) is now simply an eigenvector of the matrix M with eigenvalue $-\omega_m^2$:

$$-\omega_m^2 a_{m,j} = M_{ij} a_{m,i}. \tag{22}$$

The index m is used to label the different solutions to the above equation. In practical calculations, one truncates the series of equation (19) at a finite index $i = N$, so that one obtains a total number of N eigensolutions. The eigenvalue problem of equation (21) with finite $(N \times N)$ matrix M can be solved by means of standard linear algebra methods. Given a set of suitable basis functions, the eigenvectors and eigenvalues (or crustal eigenfrequencies) converge on the correct solutions of equation (18) for sufficiently large N (see the discussion of Section 3.5).

Orthogonality relation for elastomagnetic modes

In the limit of $N \rightarrow \infty$, the elastomagnetic eigenfunctions are

$$\bar{\boldsymbol{\xi}}_m(\boldsymbol{x}) = \sum_i a_{m,i} \boldsymbol{\Psi}_i(\boldsymbol{x}), \tag{23}$$

where we omitted the time-dependent part ${\rm e}^{{\rm i}\omega_m t}$, on both sides. The eigenfunctions $\bar{\boldsymbol{\xi}}_m$ will form a new basis for a Hilbert space of crustal displacements. We can introduce an inner product $\langle \ldots | \ldots \rangle_{\rm me}$ in which this basis is orthogonal as follows: consider a deformation $\bar{\boldsymbol{\xi}}(\boldsymbol{x}, t)$ of the crust, decomposed into a sum of eigenfunctions

$$\bar{\boldsymbol{\xi}}(\boldsymbol{x}, t) = \sum_m b_m(t) \bar{\boldsymbol{\xi}}_m(\boldsymbol{x}), \tag{24}$$

where we incorporated the harmonic time dependence in the coefficients $b_m(t)$. Since $\bar{\boldsymbol{\xi}}_m$ are the eigenmodes of the crust, the kinetic energy of the displacement field $K(\bar{\boldsymbol{\xi}})$ must be equal to the sum of kinetic energies of the individual modes $K(b_m \bar{\boldsymbol{\xi}}_m)$:

$$K\left(\bar{\boldsymbol{\xi}}(\boldsymbol{x}, t)\right) = \sum_m K\left(b_m(t) \bar{\boldsymbol{\xi}}_m(\boldsymbol{x})\right). \tag{25}$$

In the static Schwarzschild space–time of the neutron star, the conjugate time-like momentum $p_t = -E$ is a constant of geodesic motion (see e.g. Misner, Thorne & Wheeler 1973, section 25.2). In terms of the locally measured energy $E_{\rm L} = \sqrt{-g_{tt}} p^t$, the conserved 'redshifted' energy is $E = -p_t = \sqrt{-g_{tt}} E_{\rm L}$. Similarly, the kinetic energy K in terms of the locally measured kinetic energy $K_{\rm L}$ is

$$\begin{aligned} K\left(\bar{\boldsymbol{\xi}}\right) &= \sqrt{-g_{tt}} K_{\rm L}\left(\bar{\boldsymbol{\xi}}\right) \\ &= \frac{1}{2} \int_{\mathcal{V}} \sqrt{-g_{tt}} \tilde{\rho} \left| \frac{\partial \bar{\boldsymbol{\xi}}}{\partial \tau} \right|^2 {\rm d}\tilde{V} = \frac{1}{2} \int_{\mathcal{V}} \frac{\tilde{\rho}}{\sqrt{-g_{tt}}} \left| \frac{\partial \bar{\boldsymbol{\xi}}}{\partial t} \right|^2 {\rm d}\tilde{V} \\ &\equiv \frac{1}{2} \langle \partial \bar{\boldsymbol{\xi}} / \partial t | \partial \bar{\boldsymbol{\xi}} / \partial t \rangle_{\rm me}, \end{aligned} \tag{26}$$

where $\tilde{\rho} = \left(\rho + P/c^2 + B^2/4\pi c^2\right)$ is the mass density in a local Lorentz frame, and ${\rm d}\tilde{V} = \sqrt{g_{rr} g_{\phi\phi} g_{\theta\theta}} \, {\rm d}r \, {\rm d}\phi \, {\rm d}\theta$ is the locally measured space-like volume element. By substituting this expression for

the kinetic energy into equation (25), one finds that the cross-terms, $\langle \partial \bar{\boldsymbol{\xi}}_m / \partial t | \partial \bar{\boldsymbol{\xi}}_k / \partial t \rangle_{\rm me} = \omega_m \omega_k \langle \bar{\boldsymbol{\xi}}_m | \bar{\boldsymbol{\xi}}_k \rangle_{\rm me}$ with $m \neq k$, vanish. After normalizing the eigenfunctions $\bar{\boldsymbol{\xi}}_m$, so that $K(b_m \bar{\boldsymbol{\xi}}_m) = 1/2 \omega_m^2 b_m^2$, we obtain the orthogonality relation

$$\langle \bar{\boldsymbol{\xi}}_m | \bar{\boldsymbol{\xi}}_k \rangle_{\rm me} = \int_{\mathcal{V}} \frac{\tilde{\rho}}{\sqrt{-g_{tt}}} \bar{\boldsymbol{\xi}}_m \cdot \bar{\boldsymbol{\xi}}_k \mathrm{d}\tilde{V} = \delta_{mk}. \tag{27}$$

The coefficients $b_m(t)$ are now simply obtained by taking the inner product between the displacement field $\bar{\boldsymbol{\xi}}(\boldsymbol{x}, t)$ and the eigenfunctions $\bar{\boldsymbol{\xi}}_m(\boldsymbol{x})$:

$$b_m(t) = \langle \bar{\boldsymbol{\xi}}(\boldsymbol{x}, t) | \bar{\boldsymbol{\xi}}_m(\boldsymbol{x}) \rangle_{\rm me}. \tag{28}$$

In the next two sections, we give expressions for $\boldsymbol{L}_{\rm mag}$ and $\boldsymbol{L}_{\rm el}$, and we discuss our choice of basis functions $\boldsymbol{\Psi}_i$ and the resulting boundary forces (due to the no-stress boundary conditions) at the end of Section 3.2. In Section 3.3, we set up a realistic model of the magnetar crust and we calculate the corresponding elastomagnetic modes in Section 3.4, where we apply the formalism described above. In the remainder of this paper, we will focus solely on axisymmetric azimuthal displacement fields, that is, $\bar{\boldsymbol{\xi}} = \bar{\xi} \hat{e}_\phi$ (where $\hat{e}_\phi$ is the unit vector in the azimuthal direction and $\bar{\xi}$ is the displacement amplitude) and $\partial \bar{\xi} / \partial \phi = 0$.

3.1 Magnetic force density in the free crust

While the equations of Section 2 hold at arbitrary locations in the star, we will now consider magnetic forces acting on axisymmetric, azimuthal perturbations $\bar{\boldsymbol{\xi}}(r, \theta) = \bar{\xi}(r, \theta) \hat{e}_\phi$ in the 'free' crust, that is, a crust with no external stresses acting on it. This implies that to equation (17) we have to add boundary force terms arising from this no-external-stress condition. The tangential forces per unit area on both boundaries are given by

$$\begin{aligned} T_{\rm mag}(r_{\rm in} + \epsilon) - T_{\rm mag}(r_{\rm in} - \epsilon) &= T_{\rm mag}(r_{\rm in} + \epsilon), \\ T_{\rm mag}(r_{\rm out} + \epsilon) - T_{\rm mag}(r_{\rm out} - \epsilon) &= -T_{\rm mag}(r_{\rm out} - \epsilon), \end{aligned} \tag{29}$$

where $T_{\rm mag}(r)$ is the magnetic stress at r, and ϵ is an infinitesimal number. Adding the boundary terms, we obtain

$$\begin{aligned} &L_{\rm mag}(\bar{\xi}) \\ &= \sqrt{\frac{g_{tt}}{g_{\chi\chi}}} \frac{B}{4\pi c^2 \tilde{\rho} \sqrt{g_{\phi\phi}}} \frac{\partial}{\partial \chi} \left[\sqrt{\frac{g_{tt}}{g_{\chi\chi}}} g_{\phi\phi} B \frac{\partial}{\partial \chi} \left(\frac{\bar{\xi}}{\sqrt{g_{\phi\phi}}} \right) \right] \\ &\quad + \frac{1}{\tilde{\rho}} T_{\rm mag} \left[\delta(r - r_0) - \delta(r - r_1) \right], \end{aligned} \tag{30}$$

where δ is a Dirac delta function. The magnetic stress $T_{\rm mag}$ is derived by linearizing equation (12) and retaining first-order terms. One obtains

$$T_{\rm mag} = \frac{\sqrt{g_{tt} g_{\phi\phi}}}{g_{\chi\chi}} \cos\alpha \frac{B^2}{4\pi} \frac{\partial}{\partial \chi} \left(\frac{\bar{\xi}}{\sqrt{g_{\phi\phi}}} \right). \tag{31}$$

3.2 Relativistic equations for elastic forces

In the following, we use relativistic equations describing the elastic force density acting on axial perturbations in the crust as derived by Schumaker & Thorne (1983) (see also Karlovini & Samuelsson 2007), and presented in a convenient form by SA (for more details on the derivation of the following equations, we refer the reader to these two papers). As shown in SA, the equation of motion for axial perturbations in a purely elastic crust, that is, $\partial^2 \bar{\boldsymbol{\xi}} / \partial t^2 = \boldsymbol{L}_{\rm el}(\bar{\boldsymbol{\xi}})$, can be solved by expanding the displacement field $\bar{\boldsymbol{\xi}}(r, \theta, \phi)$ into vector spherical harmonics $\bar{\boldsymbol{\xi}}_{{\rm H},lm}(\theta, \phi) \propto \boldsymbol{r} \times \nabla Y_l^m$ (where Y_l^m is a spherical harmonic of degree l and order m) and corresponding radial- and time-dependent parts $\bar{\xi}_{\rm R}(r)$ and $f_{\rm T}(t)$ of the displacement field. Rewriting equation (2) of SA now gives

$$\begin{aligned} &\boldsymbol{L}_{\rm el}\left(\bar{\boldsymbol{\xi}}\right) \\ &= \frac{1}{\tilde{\rho}} \left[\frac{1}{r^3} \sqrt{\frac{g_{tt}}{g_{rr}}} \frac{\mathrm{d}}{\mathrm{d}r} \left(\sqrt{\frac{g_{tt}}{g_{rr}}} r^4 \mu \frac{\mathrm{d}}{\mathrm{d}r} \left(\frac{\bar{\xi}_{\rm R}}{r} \right) \right) \right. \\ &\quad \left. - \mu g_{tt} \frac{(l-1)(l+2)}{r^2} \bar{\xi}_{\rm R} \right] \bar{\boldsymbol{\xi}}_{{\rm H},lm} f_{\rm T}, \end{aligned} \tag{32}$$

where the metric terms g_{tt} and g_{rr} are the standard Schwarzschild metric terms, and $\mu(r)$ is the (isotropic) shear modulus. The expansion of $\bar{\boldsymbol{\xi}}$ into vector spherical harmonics leads to a particularly simple stress-free boundary condition for the radial function $\bar{\xi}_{\rm R}$:

$$\frac{\mathrm{d}}{\mathrm{d}r} \left(\frac{\bar{\xi}_{\rm R}}{r} \right) = 0, \tag{33}$$

which is valid on the inner and outer boundaries, $r = r_0$ and $r = r_1$, respectively.

We are now ready to select our basis functions $\boldsymbol{\Psi}_i$ in order to solve equation (18). It is convenient to separate $\boldsymbol{\Psi}_i$ into angular and radial parts, that is, $\boldsymbol{\Psi}_i = \boldsymbol{\Psi}_{{\rm H},i} \Psi_{{\rm R},i}$. Although our particular choice of basis is technically arbitrary, in view of the above discussion, a natural choice for the angular part $\boldsymbol{\Psi}_{{\rm H},i}$ is vector spherical harmonics of order $m = 0$ and $l = 2, 4, 6, \ldots$, etc. (we consider axisymmetric perturbations which are antisymmetric with respect to the equator),

$$\boldsymbol{\Psi}_{{\rm H},l}(\theta) = \sqrt{\frac{4\pi}{l(l+1)}} \left(\boldsymbol{r} \times \nabla Y_l^0 \right) = \sqrt{\frac{4\pi}{l(l+1)}} \frac{\mathrm{d}Y_l^0}{\mathrm{d}\theta} \hat{e}_\phi, \tag{34}$$

which are orthonormal with respect to the following inner product:

$$\langle \boldsymbol{\Psi}_{{\rm H},l} | \boldsymbol{\Psi}_{{\rm H},l'} \rangle = \int_0^\pi \boldsymbol{\Psi}_{{\rm H},l} \cdot \boldsymbol{\Psi}_{{\rm H},l'} \sin\theta \mathrm{d}\theta = \delta_{ll'}. \tag{35}$$

One tempting choice for the radial function is to use the radial eigenmodes of equation (32), $\bar{\xi}_{{\rm R},n}$ (where n is the number of radial nodes) as basis functions, that is, $\Psi_{{\rm R},n} = \bar{\xi}_{{\rm R},n}$. It turns out, however, that the expansion of the elastomagnetic displacement field (see equation 19) into elastic eigenfunctions is very inefficient. We found that better convergence is realized with

$$\begin{aligned} \Psi_{{\rm R},n}(r) &= r \sqrt{\frac{2}{r_1 - r_0}} \cos\left(\frac{\pi n (r - r_0)}{r_1 - r_0} \right) \quad \text{for } n = 1, 2, \ldots, \\ \Psi_{{\rm R},n}(r) &= r \sqrt{\frac{1}{r_1 - r_0}} \quad \text{for } n = 0, \end{aligned} \tag{36}$$

which obey equation (33), so that no extra boundary terms in $\boldsymbol{L}_{\rm el}$ are needed to preserve the stress-free condition. The basis functions of equation (36) are orthonormal with respect to the following inner product:

$$\langle \Psi_{{\rm R},n} | \Psi_{{\rm R},n'} \rangle = \int_{r_0}^{r_1} \Psi_{{\rm R},n} \Psi_{{\rm R},n'} \frac{1}{r^2} \mathrm{d}r = \delta_{nn'} \tag{37}$$

Combining equations (34) and (37) gives us a series of basis functions that we use in the next section to calculate elastomagnetic modes of the crust

$$\boldsymbol{\Psi}_{ln}(r, \theta) = \Psi_{{\rm R},n}(r) \boldsymbol{\Psi}_{{\rm H},l}(\theta), \tag{38}$$

which are orthonormal:

$$\langle \boldsymbol{\Psi}_{ln} | \boldsymbol{\Psi}_{l'n'} \rangle = \int_{r_0}^{r_1} \int_0^\pi \frac{\sin\theta}{r^2} \boldsymbol{\Psi}_{ln} \cdot \boldsymbol{\Psi}_{l'n'} \mathrm{d}\theta \, \mathrm{d}r = \delta_{ll'} \delta_{nn'}. \tag{39}$$

Note that the weight function w of equation (20) takes the form $w(r, \theta) = \sin\theta / r^2$.

3.3 The neutron star model

We assume that our star is non-rotating and neglect deformations due to magnetic pressure, which are expected to be small. Therefore, we adopt a spherically symmetric background stellar model that is a solution of the Tolman–Oppenheimer–Volkoff equation. We calculate the hydrostatic equilibrium using a SLy equation of state (Douchin & Haensel 2001; Haensel & Potekhin 2004; Haensel, Potekhin & Yakovlev 2007) (see *http://www.ioffe.ru/astro/NSG/NSEOS/*by Haensel & Potekhin for a tabulated version). The model that we use throughout this paper has a mass of $M_* = 1.4\,\mathrm{M}_\odot$, a radius $R_* = 1.16 \times 10^6$ cm, a crust thickness $\Delta R = 7.9 \times 10^4$ cm, a central density $\rho_\mathrm{c} = 9.83 \times 10^{14}\,\mathrm{g\,cm^{-3}}$ and cental pressure $P_\mathrm{c} = 1.36 \times 10^{35}\,\mathrm{dyne\,cm^{-2}}$. The crustal shear modulus μ is given by (Strohmayer et al. 1991)

$$\mu = \frac{0.1194}{1 + 0.595(173/\,\Gamma)^2}\frac{n(Ze)^2}{a}, \tag{40}$$

where n is the ion density, $a = (3/4\pi n)^{1/3}$ is the average spacing between ions and $\Gamma = (Ze)^2/ak_\mathrm{B}T$ is the Coulomb coupling parameter. We evaluate μ in the limit $\Gamma \to \infty$.

To the spherical star we add a poloidal magnetic field, which we generate as follows: we start with an Euclidean (flat) space into which we place a circular current loop of radius $r_\mathrm{cl} = 0.55R_*$ and current I and calculate the magnetic field generated by the loop (see e.g. Jackson 1998). Then we map this field on to the curved space–time of the neutron star, as discussed in Section 2. The field is singular near the current loop; however, all the field lines which connect to the crust (and thus are physically related to observable oscillations) carry finite field values. This particular field configuration is chosen as an example; there is an infinite number of ways to generate poloidal field configurations. In Fig. 1, we plot resulting shear and Alfvén velocities in the crust as a function of radial coordinate r.

3.4 Results

We now use the formalism and equations of the previous sections to calculate elastomagnetic modes of the magnetar crust. We construct

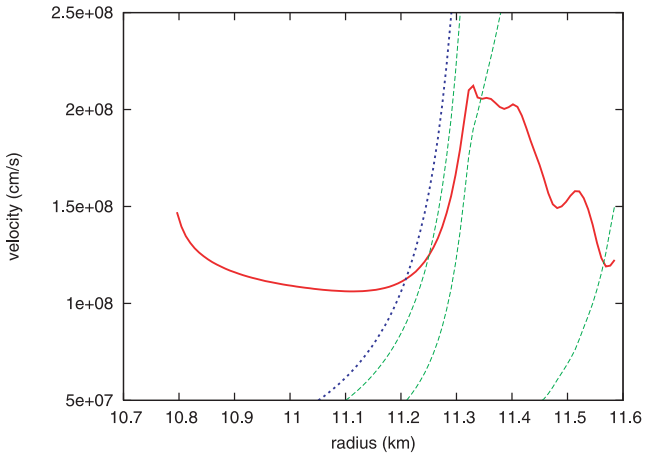

Figure 1. Shear velocity $c_\mathrm{s} = \sqrt{\mu/\rho}$ (solid line) versus Alfvén velocity $c_\mathrm{A} = \sqrt{B^2/4\pi\rho}$ for a poloidal field strength of 10^{15} G (dotted line). The dashed lines are the radial components of the Alfvén velocity, $c_\mathrm{A,rad} = c_\mathrm{A}\cos\alpha$, evaluated at (from the left-hand to right-hand side) $\theta = 69^\mathrm{o}$, 79^o and 89^o. Closer to the poles (smaller θ), the field becomes nearly radial and $c_\mathrm{A,rad} \sim c_\mathrm{A}$. The c_A curve shown in this plot is evaluated at the pole ($\theta = 0^\mathrm{o}$), but varies negligibly as a function of θ.

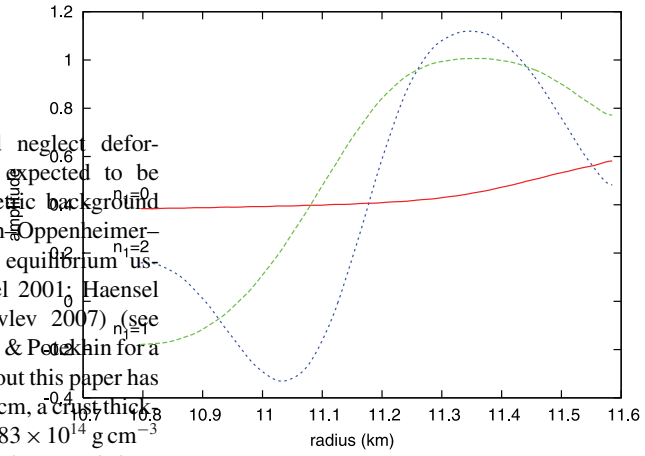

Figure 2. Radial profiles of $l_1 = 2$ elastomagnetic modes, evaluated at $\theta = 81^\mathrm{o}$. The vertical scale of individual curves is adapted for visual convenience.

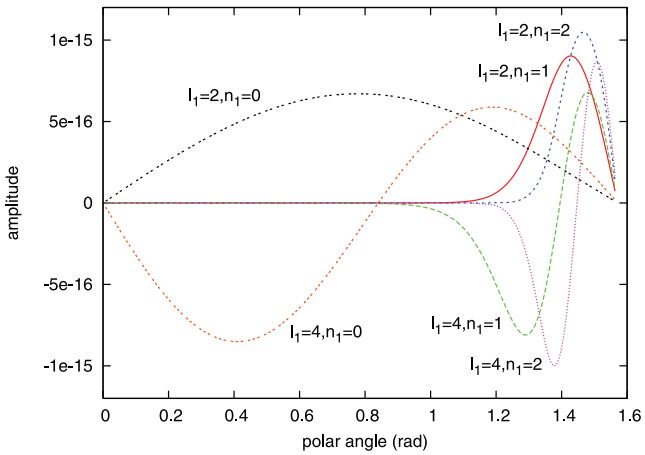

Figure 3. Examples of elastomagnetic eigenmodes for $B_\mathrm{p} = 10^{15}$ G (where B_p is the field strength at the magnetic pole), as a function of the polar angle θ, evaluated at the crust–core interface. The $n_1 = 0$ modes are nearly unaffected by the magnetic field and are spread out over the crust, whereas the $n_1 > 0$ modes are affected strongly by the magnetic field, and are confined to regions near the equator, where the field is horizontal.

a basis from N_n radial functions $\Psi_{\mathrm{R},n}(r)$ (see equation 36) with index $n = 0, 1, \ldots, N_n - 1$, and N_l angular functions $\mathbf{\Psi}_{\mathrm{H},l}(\theta)$ (see equation 34) with even index $l = 2, 4, \ldots, 2N_l$. These functions provide a set of $N_n \times N_l$ linearly independent basis functions $\mathbf{\Psi}_{ln}$. Using this basis, we solve the matrix equation (22), and reconstruct the normal modes according to equation (19).

Radial and horizontal cross-sections of a selection of eigenmodes are plotted in Figs 2 and 3, and Table 1 contains a list of frequencies. These results are based on a stellar model with a poloidal field strength of 10^{15} G at the magnetic pole. For the calculation, we used $N_n = 35$ radial basis functions and $N_l = 35$ angular basis functions. We labelled the modes with integer indices $n_1 = 0, 1, 2, \ldots$ and $l_1 = 2, 4, 6, \ldots$, where n_1 is defined as the number of nodes along the r-axis and $l_1 + 1$ is the number of nodes along the θ-axis (including the poles). Note that the index l_1, in contrast to l, does not signify a spherical harmonic degree since the angular dependence of the elastomagnetic modes differs from pure spherical harmonics. However, there is a connection between the two indices: the elastomagnetic mode of degree l_1 and order n_1 can be interpreted as the magnetically perturbed elastic mode of the same

Table 1. The eigenfrequencies of the non-magnetic crust (second column) versus the eigenfrequencies of the magnetized crust (third column), with a magnetic field of 10^{15} G at the polar surface. The elastomagnetic frequencies were calculated using a basis of 35×35 basis functions Ψ_{ln}.

Mode indices	Elastic modes ($B = 0$ G)	Elastomagnetic modes ($B = 10^{15}$ G)
$n_1 = 0, l_1 = 2$	27.42 Hz	27.61 Hz
$n_1 = 0, l_1 = 4$	58.16 Hz	59.14 Hz
$n_1 = 0, l_1 = 6$	86.69 Hz	88.13 Hz
$n_1 = 0, l_1 = 8$	114.7 Hz	116.5 Hz
$n_1 = 1, l_1 = 2$	895.9 Hz	954.1 Hz
$n_1 = 1, l_1 = 4$	897.4 Hz	985.7 Hz
$n_1 = 1, l_1 = 6$	899.7 Hz	1001.4 Hz
$n_1 = 1, l_1 = 8$	902.8 Hz	1003.4 Hz
$n_1 = 2, l_1 = 2$	1474.6 Hz	1607.1 Hz
$n_1 = 2, l_1 = 4$	1475.7 Hz	1664.4 Hz
$n_1 = 2, l_1 = 6$	1477.5 Hz	1708.1 Hz
$n_1 = 2, l_1 = 8$	1479.9 Hz	1740.4 Hz

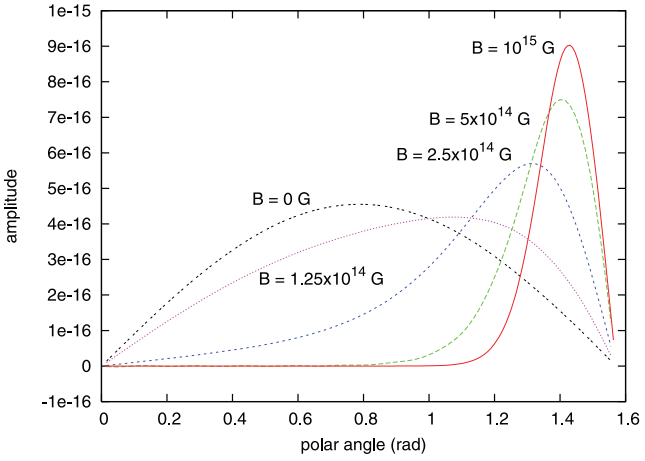

Figure 4. Angular geometry of the $l_1 = 2, n_1 = 1$ crustal mode (at the crust–core interface), as a function of the magnetic field strength. For zero magnetic field, the curve is identical to the $l = 2$ vector spherical harmonic $\Psi_{\mathrm{H},l}(\theta)$. As the field strength increases, the crustal motion becomes gradually more confined towards the equator.

order and (spherical harmonic) degree. More precisely, if one gradually increases the magnetic field strength, the n, l elastic mode transforms into the elastomagnetic mode of the same indices, $n_1 = n$ and $l_1 = l$ (see Fig. 4). It is interesting to note (see Figs 3 and 4) that as the field strength increases, modes with $n_1 > 0$ become more and more confined to a narrow region near the equator (a similar effect was recently observed in the grid-based simulations of Gabler et al. 2011b). In the equatorial regions, the horizontal field creates a magnetic tension-free cavity for modes with radial nodes, which are reflected back towards the equator at higher latitudes where the field becomes more radial.[2] The $n_1 = 0$ modes, however, having no radial nodes, are virtually insensitive to the magnetic field and are therefore not confined to low latitudes. The field strength dependence of the eigenfrequencies, illustrated in Fig. 5, is qualitatively similar to results obtained by other authors (see Carroll et al. 1986; Piro 2005; Sotani et al. 2007). As we increase the field strength, we find that the increase in frequency $\delta\omega$ for $n_1 = 0$ modes scales weakly with B, that is, $\delta\omega \propto B^2$. For modes with $n_1 > 0$, $\delta\omega \propto B^2$ if $B < 5 \times 10^{13}$ G, and $\delta\omega \propto B$ if $B > 5 \times 10^{13}$ G.

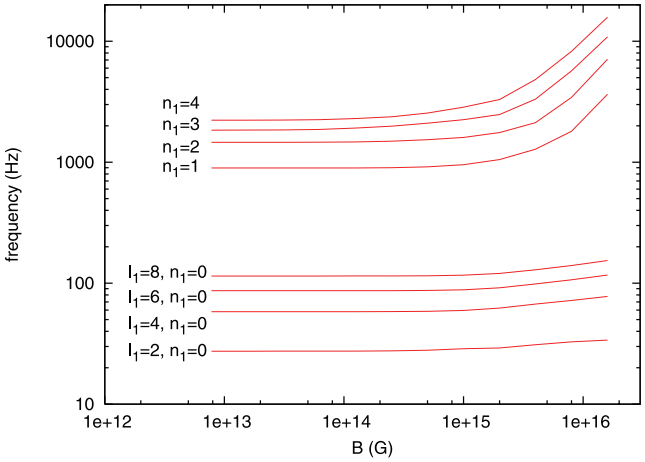

Figure 5. Frequencies as a function of B. For $n_1 > 0$, the frequencies of (low) l_1 modes nearly coincide and are therefore collectively indicated with their n_1 value, that is, $n_1 = 1, 2, \ldots$, etc. Note that at high field strengths, the $n_1 > 0$ frequencies collectively behave as $\omega \propto B$.

As a test, we compared the eigenfrequencies and eigenmodes for zero field, $B = 0$, to those obtained by a direct integration of the elastic equation of motion equation(32).[3] We find that both frequencies and wavefunctions obtained by the series expansion method converge rapidly[4] to real values, obtained by integration of equation (32). For example, for $N_n = 10$, $n_1 = 0$ elastic frequencies have a typical error of 0.02 per cent, while frequencies for modes $n_1 < 4$ are well within 1 per cent accuracy. In Fig. 6 , we plot elastic eigenfunctions, obtained by both methods. The solutions from the series expansion method with $N_n = 10$ radial basis functions are nearly indistinguishable from the solutions obtained by direct integration.

For the full elastomagnetic equation of motion, equation (18) with a magnetic field strength of 10^{15} G at the pole, we tested the convergence of resulting eigenfrequencies by increasing the number of basis functions, N_n and N_l (see Fig. 7). We find that, compared to the non-magnetic case, a significant number N_n of radial functions and N_l angular functions are required to get acceptable convergence to stable results. The large number of required radial basis functions can be understood from the fact that the magnetic acceleration L_B (equation 30) contains delta functions, arising from the boundary terms. Obviously, one needs many radial basis functions to obtain an

[2] A similar effect is well known from the study of waveguides: as the waveguide gets narrower (i.e. as its transverse frequency increases), the propagating wave may become evanescent in the longitudinal direction and be reflected.

[3] The latter works as follows: one starts by assuming harmonic time dependence for the displacement $\vec{\xi}$, so that $L_{\mathrm{el}}(\vec{\boldsymbol{\xi}}) = -\omega^2\vec{\boldsymbol{\xi}}$. Dropping the angular- and time-dependent parts of $\vec{\boldsymbol{\xi}}$ on both sides of the equation, one is left with an equation for $\vec{\xi}_{\mathrm{R}}$, which is integrated from the bottom of the crust, with corresponding boundary condition, to the surface. This is repeated for different ω until the surface boundary condition is satisfied, that is, one has found an eigenmode. By repeating this procedure with gradually increasing ω, one obtains a series of eigenmodes and eigenfrequencies.

[4] Note that in the purely elastic case, l is a good quantum number and the angular basis functions $\boldsymbol{\Psi}_{\mathrm{H},l}(\theta)$ are already solutions to the elastic eigenmode equation. Therefore, for a given $l_1 = l$, only the series with the radial basis functions needs to be considered.

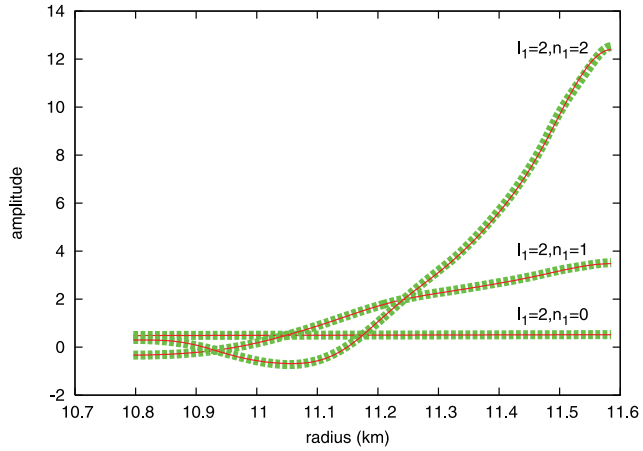

Figure 6. Elastic crustal modes obtained through integration of the elastic equation of motion (thick dashed curves), and the same modes obtained by the series expansion method (overplotted by the thin solid curve), using $N_n = 10$ radial basis functions.

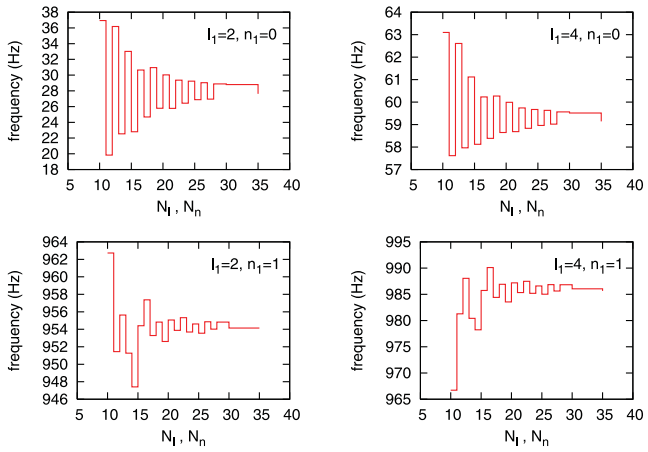

Figure 7. Demonstration of convergence for elastomagnetic frequencies for low-order, low-degree modes as a function of N_n and N_l, where we took $N_n = N_l$. The actual number of basis functions, $N = N_n \times N_l$, is the square of the value along the x-axis.

acceptable sampling of these boundary terms. The number of computational operations, however, is a steep function of the number of basis functions [approximately $\propto (N_l \times N_n)^3$], so that computations with large N_l and N_n can become unpractical in ordinary workstations. Although this limits the number of basis functions in our calculations, we find that for N_l, $N_n \sim 35$, the scatter in frequencies is typically $\lesssim$1 per cent for most modes (Fig. 7), and the eigenfunctions $\bar{\xi}_m$ reproduce the orthogonality relation (27) with good precision.

4 CORE CONTINUUM AND CRUST–CORE COUPLING

4.1 The continuum

The equation of motion in this case is simply the Alfvén wave equation

$$\frac{\partial^2 \xi(\psi, \chi)}{\partial t^2} = L_{\rm mag}\left[\xi(\psi, \chi)\right], \tag{41}$$

where t denotes the Schwarzschild time-coordinate. The operator $L_{\rm mag}$ is given in equation (17), which we repeat here for convenience:

$$L_{\rm mag}\left[\xi(\psi, \chi)\right] = \frac{1}{\tilde{\rho} c^2} \sqrt{\frac{g_{tt}}{g_{\chi\chi}}} \frac{B}{4\pi \sqrt{g_{\phi\phi}}} \frac{\partial}{\partial \chi} \left[\sqrt{\frac{g_{tt}}{g_{\chi\chi}}} g_{\phi\phi} B \frac{\partial}{\partial \chi} \left(\frac{\xi}{\sqrt{g_{\phi\phi}}} \right) \right]. \tag{42}$$

Here g_{tt}, $g_{\chi\chi}$ and $g_{\phi\phi}$ are the metric terms corresponding to the system of coordinates defined in Section 2.

For determining the spectrum of the core continuum, the appropriate boundary conditions are $\xi(\chi = \chi_{\rm c}) = 0$, where $\chi_{\rm c}(\phi)$ marks the location of the crust–core interface. The full significance of this boundary condition will become apparent later in this section when we develop the analysis for the crust–core interaction (see also section 4.2 in Paper I). With this boundary condition, equation (41) constitutes a Sturm–Liouville problem on each separate flux surface ψ. Using the stellar structure model and magnetic field configuration described in Section 3.3, we can calculate the eigenfunctions and eigenfrequencies for each flux surface ψ. The reflection symmetry of the stellar model and the magnetic field with respect to the equatorial plane assures that the eigenfunctions of equation (41) are either symmetric or antisymmetric with respect to the equatorial plane. We can therefore determine the eigenfunctions by integrating equation (41) along the magnetic field lines from the equatorial plane $\chi = 0$ to the crust–core interface $\chi = \chi_{\rm c}(\psi)$. Let us consider the odd modes here for which $\xi(0) = 0$, and solve equation (41) with the boundary condition $\xi(\chi_{\rm c}) = 0$ at the crust–core interface; for even modes, the boundary condition is $\mathrm{d}\xi(0)/\mathrm{d}\chi = 0$. We find the eigenfunctions by means of a shooting method; using fourth-order Runge–Kutta integration, we integrate from $\chi = 0$ to $\chi_{\rm c}$. The correct eigenvalues σ_n and eigenfunctions $\xi_n(\chi)$ are found by changing the value of σ until the boundary condition at ξ_n is satisfied. In this way, we gradually increase the value of σ until the desired number of harmonics is obtained. In Fig. 8, we show a typical resulting core continuum. The continuum is piece-wise, and covers the domains $\sigma = [41.8, 67.5]$ Hz and $\sigma = [91.4, \infty)$ Hz. Gaps, such as the one between 67.5 and 91.4 Hz in Fig. 8, are a characteristic feature of the type of poloidal field that we employ in this paper, and typically occur at low frequencies (i.e. $\sigma < 150$ Hz). As we discuss in

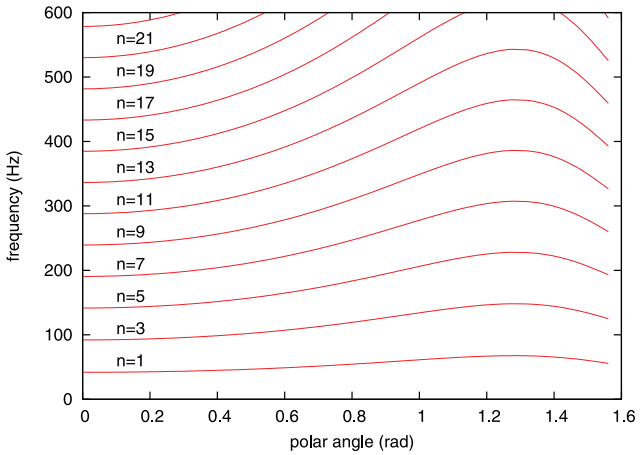

Figure 8. The curves show the Alfvén frequencies σ_n as a function of the angle $\theta(\psi)$, the polar angle at which the flux surface ψ intersects the crust. Since we are only considering odd crustal modes, the only Alfvén modes that couple to the motion of the star are the ones with an odd harmonic number n. This particular continuum was calculated using a poloidal field with a surface value of $B = 10^{15}$ G at the poles.

Section 4.3, they may give rise to strong low-frequency QPOs (see also Paper I and Colaiuda & Kokkotas 2011).

According to Sturm–Liouville theory, the normalized eigenfunctions ξ_n of equation (41) form an orthonormal basis with respect to the following inner product:

$$\langle \xi_m, \xi_n \rangle = \int_0^{\chi_c} r(\chi)\, \xi_m(\chi)\, \xi_n(\chi)\, \mathrm{d}\chi = \delta_{m,n}, \tag{43}$$

where $\delta_{m,n}$ is the Kronecker delta. Noting that the operator $L_{\rm mag}(\xi)$ is in Sturm–Liouville form, one reads off the weight function $r(\chi)$:

$$r = \sqrt{\frac{g_{\chi\chi}}{g_{tt}}}\frac{4\pi\tilde{\rho}}{B_\chi}. \tag{44}$$

We have checked that the solutions $\xi_n(\chi)$ satisfy the orthogonality relations.

4.2 Equations of motion for the coupled crust and core

We are now ready to compute the coupled crust–core motion. In contrast to L07 and Paper I, where the crust was assumed to be an infinitely thin spherical elastic shell, we shall here adopt a crust of finite thickness with realistic structure. We label the latitudinal location by the flux surface ψ intersecting the crust–core interface, and consider the crustal axisymmetric displacements $\bar{\xi}_\phi(\psi, r)$, where r is the radial Schwarzschild coordinate. In the MHD approximation, the magnetic stresses enforce a no-slip boundary condition at the crust–core interface (at $r = r_0$ in the Schwarzschild coordinates of the crust, or $\chi_{\rm c}$ in the flux coordinates of the core), such that $\xi(\psi, \chi_{\rm c}) = \bar{\xi}(\theta(\psi), r_0)$ instead of $\xi(\psi, \chi_{\rm c}) = 0$. It is useful to make the following substitution:

$$\zeta(\psi, \chi) \equiv \xi(\psi, \chi) - \bar{\xi}(\theta(\psi), r_0)\, w(\psi, \chi), \tag{45}$$

where we choose the function $w(\psi, \chi)$ so that (i) it corresponds to the static displacement in the core and hence satisfies $L_{\rm mag}(w(\psi, \chi)) = 0$, and (ii) $w(\psi, \chi_{\rm c}) = 1$. From the definition of the operator F, it follows that for the odd modes

$$w(\psi, \chi) = \sqrt{g_{\phi\phi}} \int_0^{\chi} \sqrt{\frac{g_{\chi\chi}}{g_{tt}}}\, \frac{K(\psi)}{g_{\phi\phi} B(\psi, \chi')}\, \mathrm{d}\chi'. \tag{46}$$

Here the constant $K(\psi)$ is chosen such that $w(\psi, \chi_{\rm c}) = 1$. The new quantity ζ from equation (45) now satisfies the boundary condition $\zeta(\psi, \chi_{\rm c}) = 0$ and can be expanded into the Alfvén normal modes ξ_n which satisfy the same boundary conditions.

We now proceed by substituting equation (45) into equation (41), thus obtaining a simple equation of motion for ζ:

$$\frac{\partial^2 \zeta(\psi, \chi)}{\partial t^2} - L_{\rm mag}(\zeta(\psi, \chi)) = -w(\psi, \chi)\, \frac{\partial^2 \bar{\xi}(\theta(\psi), r_0)}{\partial t^2}. \tag{47}$$

We expand ζ and w into a series of ξ_n:

$$\zeta(\psi, \chi, t) = \sum_n a_n(\psi, t)\, \xi_n(\psi, \chi), \tag{48}$$

$$w(\psi, \chi) = \sum_n c_n(\psi)\, \xi_n(\psi, \chi). \tag{49}$$

Using these expansions, equation (47) reduces to the following equations of motion for the eigenmode amplitudes a_n:

$$\frac{\partial^2 a_n(\psi)}{\partial t^2} + \sigma_n^2(\psi)\, a_n(\psi) = -c_n(\psi)\, \frac{\partial^2 \bar{\xi}(\psi, r_0)}{\partial t^2}. \tag{50}$$

These equations show how the core Alfvén modes are driven by the motion of the crust. To close the system, we must address the motion of the crust driven by the hydromagnetic pull from the core:

$$\frac{\partial^2 \bar{\xi}}{\partial t^2} = L_{\rm crust}\left(\bar{\xi}\right) - \tfrac{1}{\tilde{\rho}}\left[\frac{g_{tt}}{g_{\chi\chi}}\frac{\sqrt{g_{\phi\phi}}B^2}{4\pi c^2}\cos\alpha\,\frac{\partial}{\partial\chi}\left(\frac{\xi}{\sqrt{g_{\phi\phi}}}\right)\right]\delta(r - r_0). \tag{51}$$

The expression between the square brackets is the hydromagnetic stress from the stellar core acting on the crust, α is the angle between the magnetic field line and the radial coordinate of the star, and $L_{\rm crust}\left(\bar{\xi}\right) = L_{\rm mag}\left(\bar{\xi}\right) + L_{\rm el}\left(\bar{\xi}\right)$ is the acceleration of the crustal displacement due to magnetic and elastic stresses (see Section 3). We can rewrite this in terms of the coefficients, using equation (45), the definition of w, and the expansions and orthogonality relations of equations (27) and (28), as

$$\frac{\partial^2 b_j}{\partial t^2} + \Omega_j^2 b_j = -\int_0^{\pi} \frac{\sqrt{g_{rr}g_{tt}}}{g_{\chi\chi}}\frac{B^2}{2c^2}\cos\alpha\left(\sum_n a_n\frac{\partial\xi_n}{\partial\chi} + \sqrt{\frac{g_{\chi\chi}}{g_{tt}}}\frac{K}{B\sqrt{g_{\phi\phi}}}\sum_i b_i\bar{\xi}_i\right)\bar{\xi}_j\Big|_{r=r_0} r_0^2\sin\theta\,\mathrm{d}\theta, \tag{52}$$

where the coefficients $b_j(t)$ are crustal mode amplitudes defined in equations (24) and (28). Up to this point the derived equations of motion for the crust and the fluid core are exact. Note that, as a consequence of the crust–core coupling, equation (53) describing the evolution of $b_j(t)$ contains a term proportional to b_j on the right-hand side. This term enters due to the static fluid displacement $w\bar{\xi}$ corresponding to the jth crustal mode, and effectively loads this mode with tension. The 'tension-loaded' frequency $\tilde{\Omega}_j$ of the jth crustal mode is obtained by moving the term proportional to b_j to the left-hand side of equation (53):

$$\tilde{\Omega}_j^2 = \Omega_j^2 + \int_0^{\pi}\sqrt{\frac{g_{rr}}{g_{\chi\chi}}}\frac{BK}{2c^2}\cos\alpha\bar{\xi}_j^2 r\Big|_{r=r_0}\mathrm{d}\theta. \tag{53}$$

In the appendix, we use these 'tension-loaded' frequencies to calculate theoretical damping rates of crustal modes.

We are now ready to discretize the continuum by converting the integral of equation (51) into a sum over N points θ_i. In order to avoid the effect of phase coherence (see Section 3) which caused drifts in the results of L07, we sample the continuum randomly over the θ interval $[0, \pi/2]$. In the following, functional dependence of the coordinate ψ or $\theta(\psi)$ is substituted by the discrete index i which denotes the ith flux surface:

$$\frac{\partial^2 b_j}{\partial t^2} + \Omega_j^2 b_j = -\sum_i \frac{\sqrt{g_{rr,i}g_{tt,i}}}{g_{\chi\chi,i}}\frac{B_i^2}{2c^2}\cos\alpha_i\left(\sum_{n,i} a_{n,i}\frac{\partial\xi_{n,i}}{\partial\chi} + \sqrt{\frac{g_{\chi\chi,i}}{g_{tt,i}}}\frac{K_i}{B_i\sqrt{g_{\phi\phi,i}}}\sum_m b_m\bar{\xi}_{m,i}\right)\bar{\xi}_{j,i}\Big|_{r=r_0} r_0^2\sin\theta_i\Delta\theta_i \tag{54}$$

$$\frac{\partial^2 a_{nk}}{\partial t^2} + \sigma_{nk}^2 a_{nk} = -c_{nk}\sum_j \frac{\partial^2 b_j}{\partial t^2}\bar{\xi}_{j,k}\,. \tag{55}$$

These are the equations that fully describe dynamics of our magnetar model. As with the toy model from Section 2 we integrate them using a second-order leap-frog scheme which conserves the total energy to high precision. As a test we keep track of the total energy

of the system during the simulations. Further we have checked our results by integrating equations (53) and (55) with the fourth-order Runge–Kutta scheme for several runs and found good agreement with the leap-frog integration.

4.3 Results

Based on the results of Paper I, we expect the following dynamical characteristics to occur:

(i) Crustal modes with frequencies that are inside the continuum should undergo resonant absorption, that is, if such a mode couples efficiently to continuum Alfvén modes of the core with similar frequencies, its motion will be damped on rather short time-scales. In the appendix, we analytically investigate the efficiency of this coupling and the resulting damping time-scales.

(ii) Late-time behaviour of the system will show oscillations near the edges of the continuum; the edge modes.

(iii) Gaps, as present in the continuum of Fig. 8, will give rise to two types of QPOs: first, crustal modes which are inside these gaps will remain undamped, although slightly shifted in frequency due to the interaction with the continuum[5]; and, secondly, edge modes near the edges of the gaps may occur.

All of these characteristics were observed in simulations of Paper I, and we expect them to occur in this work.

We consider 16 crustal modes, that is, $(n, l) = (0, 2), (0, 4), (0, 6), (0, 8), (0, 10), (0, 12), (0, 14), (0, 16), (0, 18), (0, 20), (1, 2), (1, 4), (1, 6), (1, 8), (1, 10)$ and $(1, 12)$. We couple these crustal modes to 9000 continuum oscillators, that is, 300 different flux surfaces, each with 30 Alfvén overtones. We start the simulation by initializing the crustal mode amplitudes $b_j = 1$ for all crustal modes, while keeping the continuum oscillators relaxed ($a_{ni} = 0$), and evolve the system for 52 s in time.

In Table 2, we list the 'free' crustal frequencies Ω and 'tension-loaded' frequencies $\tilde{\Omega}$ for the 16 modes considered in our simulation. The last column of Table 2 contains the corresponding theoretically calculated damping rates (see Appendix A). In Figs 9 and 10, we show power spectra which were calculated using the data of the last 26 s of the simulation.Displacement of the $l_1 = 2$, $n_1 = 1$ mode is shown in Fig. 11.

Table 2. Frequencies Ω of the 'free' crustal modes (second column), and 'tension-loaded' frequencies $\tilde{\Omega}$ due to the crust–core coupling (third column; see equation 53). The resonant damping time-scales τ_d (see Appendix A) are given in the fourth column. The $n_1 = 0, l_1 = 2, 4$ modes are shifted into the 'gap' (in the interval $\sigma = [67.5, 91.4]$ Hz) and are therefore undamped. The long damping time of the $n_1 = 0, l_1 = 12$ crustal mode is due to the fact that the only resonant Alfvén layer nearly coincides with a crustal node.

Mode indices	Crustal frequencies Ω (Hz)	Tension-loaded frequencies $\tilde{\Omega}$ (Hz)	Damping time τ_d (ms)
$n_1 = 0, l_1 = 2$	27.61	71.10	∞
$n_1 = 0, l_1 = 4$	59.14	86.49	∞
$n_1 = 0, l_1 = 6$	88.13	107.6	6.2
$n_1 = 0, l_1 = 8$	116.5	131.6	0.47
$n_1 = 0, l_1 = 10$	144.7	157.0	0.53
$n_1 = 0, l_1 = 12$	172.7	183.0	287
$n_1 = 0, l_1 = 14$	200.6	209.5	0.67
$n_1 = 0, l_1 = 16$	228.5	236.3	1.3
$n_1 = 0, l_1 = 18$	256.3	263.3	0.97
$n_1 = 0, l_1 = 20$	284.1	290.4	0.83
$n_1 = 1, l_1 = 2$	954.1	955.0	5.8
$n_1 = 1, l_1 = 4$	985.7	986.7	11.4
$n_1 = 1, l_1 = 6$	1001.4	1002.4	1.4
$n_1 = 1, l_1 = 8$	1003.4	1004.5	3.3
$n_1 = 1, l_1 = 10$	1006.5	1007.5	2.7
$n_1 = 1, l_1 = 12$	1010.5	1011.6	2.5

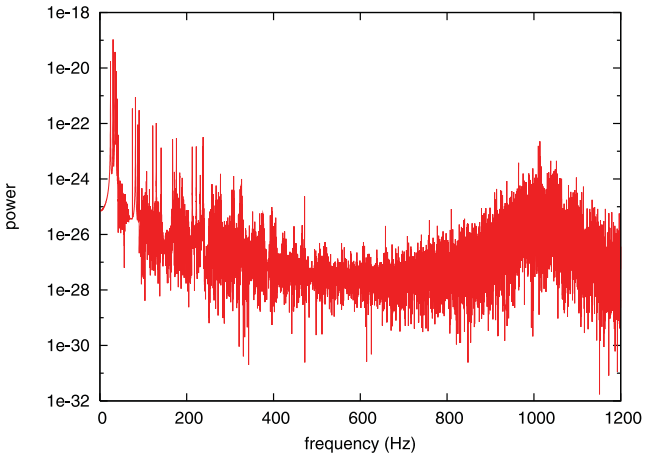

Figure 9. Power spectrum of the crustal motion.

5 DISCUSSION

In this paper, we have laid out the spectral formalism for computation of general relativistic torsional magnetar oscillations. This method is efficient; a typical simulation of 50 s of the magnetar dynamics (i.e. up to tens of thousands of the oscillatory periods) takes only a few hours of an ordinary workstation. The second-order symplectic leap-frog scheme ensures that the energy of the system is conserved with very high accuracy. Our simulations allow us to investigate which of the oscillatory behaviour is long-lived enough ($\sim$100 s) to be relevant to the observations of QPOs in the tails of giant SGR flares (Israel et al. 2005; Strohmayer & Watts 2006).

The results from our simulations are qualitatively in agreement with earlier results in Paper I. In particular, the presence of undamped crustal motion in gaps of the Alfvén continuum was established both analytically and in our numerical simulations, in contrast to recent results by Gabler et al. (2011b), where the authors report in some detail the strong damping of an elastic crustal mode inside a gap. We argue that this discrepancy might be due to the fact that Gabler et al., while considering stronger magnetic fields, couple the entire core mass, including the neutrons, to the Alfvén modes. As a result, the effective mass of the Alfvén modes is a factor of $\sim$20 greater than ours, imposing a frequency shift on the crustal mode, which may well push it out of the gap.

One of the puzzling features of the observations is several high-frequency QPOs above 600 Hz (Watts & Strohmayer 2006). The thin-crust models of Paper I had strongly suggested that crustal modes of such high frequency should be subject to the strong resonant absorption in the core, even if the core's Alfvén modes do

[5] The presence of 'gap modes' like the ones found in Paper I was recently confirmed by Colaiuda & Kokkotats (2011).

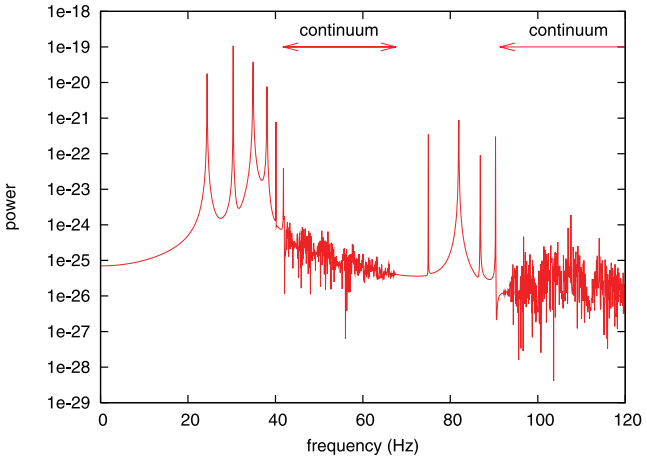

Figure 10. The same power spectrum, but closed up. The position of the continuum is indicated by the arrows.

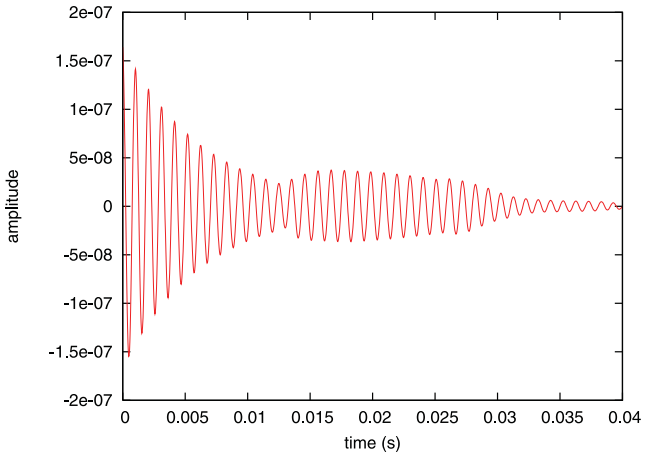

Figure 11. Displacement of the $l_1 = 2$, $n_1 = 1$ mode. The theoretically calculated damping time $\tau_d = 5.8 \times 10^{-3}$ s. Note the transient increase in the mode amplitude. This is due to the initial Alfvén wavetrain, which is reflected at the equator.

not form a mathematical continuum.[6] In accordance with results of Gabler et al. (2011b), we found that some crustal modes are confined to the regions in the crust where the magnetic field is nearly horizontal. Because of this, the coupling to the Alfvén modes in the core is reduced relative to the coupling strength estimated in Paper I; however, the coupling is still large enough for the mode energy to be drained on a time-scale small compared to the observed QPOs ($\tau_d \ll 100$ s). Thus, it is still hard to understand the high-frequency QPOs (>600 Hz) in terms of axial oscillations of the star. An interesting alternative might be to consider polar Alfvén oscillations. The polar oscillations studied by Sotani & Kokkotas (2009) form a discrete set of modes with frequencies of several hundreds of Hz and may be interesting candidates for high-frequency QPOs if their coupling to other Alfvén modes turns out to be weak.

[6] This is because the frequencies of even discrete Alfvén modes form a grid, whose characteristic spacing is much less than 600 Hz. At such high frequencies, the grid acts dynamically as a continuum (see Paper I for a more detailed discussion).

ACKNOWLEDGMENTS

This research was supported, in part, by the Leiden Observatory and the Lorentz Institute through internal grants. We thank the referee, Prof. Kostas Kokkotas, for useful comments and suggestions. MvH thanks the Monash School of Physics, where part of this research was completed, for hospitality during his extensive visit.

REFERENCES

Barat C. et al., 1983, A&A, 126, 400
Carroll B. W., Zweibel E. G., Hansen C. J., McDermott P. N., Savedoff M. P., Thomas J. H., van Horn H. M., 1986, ApJ, 305, 767
Cerdá-Durán P., Stergioulas N., Font J., 2009, MNRAS, 397, 1607
Colaiuda A., Kokkotas K. D., 2011, MNRAS, 414, 3014
Colaiuda A., Beyer H., Kokkotas K. D., 2009, MNRAS, 396, 1441
Douchin F., Haensel P., 2001, A&A, 380, 151
Duncan R. C., 1998, ApJ, 498, L45
Gabler M., Cerdá Durán P., Font J. A., Müller E., Stergioulas N., 2011a, MNRAS, 410, L37
Gabler M., Cerdá Durán P., Stergioulas N., Font J. A., Müller E., 2011b, preprint (arXiv:1109.6233)
Glampedakis K., Samuelsson L., Andersson N., 2006, MNRAS, 371, L74
Goedbloed J. P. H., Poedts S., 2004, Principles of Magnetohydrodynamics. Cambridge Univ. Press, Cambridge
Goldreich P., Reisenegger A., 1992, ApJ, 395, 250
Gruzinov A., 2008, preprint (arXiv:0812.1570)
Haensel P., Potekhin A. Y., 2004, A&A, 428, 191
Haensel P., Potekhin A. Y., Yakovlev D. G., 2007, Neutron Stars 1: Equation of State and Structure. Springer, New York
Israel G. L. et al., 2005, ApJ, 628, L53
Jackson J. D., 1998, Classical Electrodynamics, 3rd edn. Wiley, New York
Karlovini M., Samuelsson L., 2007, Class. Quantum Gravity, 24, 3171
Kouveliotou C. et al., 1999, ApJ, 510, L115
Landau L. D., Lifshitz E. M., 1976, Mechanics, 3rd edn. Pergamon Press, Oxford
Lee U., 2008, MNRAS, 385, 2069
Levin Y., 2006, MNRAS, 368, L35 (L06)
Levin Y., 2007, MNRAS, 377, 159 (L07)
Mastrano A., Melatos A., Reisenegger A., Akgün T., 2011, MNRAS, , 417, 2288
Misner C. W., Thorne K. S., Wheeler J. A., 1973, Gravitation. W. H. Freeman & Co., San Francisco
Piro A. L., 2005, ApJ, 634, L153
Poedts S., Hermans D., Goossens M., 1985, A&A, 151, 16
Samuelsson L., Andersson N., 2007, MNRAS, 374, 256 (SA)
Schumaker B. L., Thorne K. S., 1983, MNRAS, 203, 457
Sotani H., Kokkotas K. D., 2009, MNRAS, 395, 1163
Sotani H., Kokkotas K. D., Stergioulas N., 2007, MNRAS, 375, 261
Sotani H., Kokkotas K. D., Stergioulas N., 2008, MNRAS, 385, L5
Steiner W., Watts A. L., 2009, Phys. Rev. Lett., 103r1101S
Strohmayer T. E., Watts A. L., 2005, ApJ, 632, L111
van Hoven M. B., Levin Y., 2011, MNRAS, 410, 1036 (Paper I)
Watts A. L., Reddy S., 2007, MNRAS, 379, L63
Watts A. L., Strohmayer T. E., 2006, ApJ, 637, L117

APPENDIX A: DAMPED MODES

Now we explore the phenomenon of resonant absorption which occurs in a system where a harmonic oscillator is coupled to a continuum of oscillators. Our aim is to find an analytic estimate for the rate at which the energy of such an oscillator is transferred to the continuum. The objective of this section and the method that we follow are analogous to a derivation of quantum mechanical Fermi's golden rule, which gives the transition rate from one quantum mechanical eigenstate to a continuum of states.

Consider the coupled crust–core dynamics of Section 4. The forced motion of the core Alfvén modes due to the acceleration of the crust is

$$\ddot{a}_n(\psi) + \sigma_n^2(\psi) a_n(\psi) = -c_n(\psi)\ddot{\bar{\xi}}(\psi, r_0), \tag{A1}$$

where $a_n(\psi)$ is the displacement of the nth core Alfvén harmonic on the flux surface ψ with frequency σ_n, $\ddot{\bar{\xi}}(\psi, r_0)$ is the acceleration of the crust at the location where the flux surface ψ intersects the crust, and $c_n(\psi) = \langle w(\psi, \chi), \xi_n \rangle$ is a coupling constant (see equation 49). Suppose that we keep the system initially fixed in a position where the crust is displaced with amplitude $b_{m,0}$ according to the mth eigenmode, that is, $\bar{\xi} = b_{m,0}\bar{\xi}_m$, and the continuum oscillators are relaxed; $a_n(\psi) = 0$. At time $t = 0$ we release the crust which starts oscillating at the 'tension-loaded' frequency $\tilde{\Omega}_m$. Suppose that the damping time-scale $\tau_{\mathrm{d},m}$ of the crustal mode is much larger than its period $\tau_m = 2\pi/\tilde{\Omega}_m$, then the crust oscillates at roughly constant amplitude, that is, $b_m(t) \approx b_{m,0}\cos\tilde{\Omega}_m t$. This motion forces the Alfvén oscillators according to

$$\ddot{a}_n(\psi) + \sigma_n^2(\psi) a_n(\psi) = c_n(\psi)\tilde{\Omega}_m^2 b_{m,0}\bar{\xi}_m(\psi, r_0)\cos\tilde{\Omega}_m t. \tag{A2}$$

One can solve the time-evolution of the oscillator $a_n(t)$ using standard techniques (see e.g. Landau & Lifshitz 1976, section 22). After a time t the energy per flux surface $\mathcal{E}_n(\psi) = 1/2(\dot{a}_n^2 + \sigma_n^2 a_n^2)$ absorbed by the oscillator is

$$\mathcal{E}_n(\psi, t) = \frac{1}{2}c_n^2(\psi)\tilde{\Omega}_m^4 b_{m,0}^2\bar{\xi}_m^2(\psi, r_0)\left|\int_0^t \cos\tilde{\Omega}_m t' \mathrm{e}^{-\mathrm{i}\sigma_n t'}\mathrm{d}t'\right|^2. \tag{A3}$$

It is easy to verify that at late times the term between the vertical lines in equation (A3) becomes narrowly peaked around $\sigma_n = \tilde{\Omega}_m$, so that the bulk of energy is transported to oscillators which are in (near) resonance with the crust. The average rate of energy (per flux surface) transfer $\langle\dot{\mathcal{E}}_n(\psi, t)\rangle$ from the crust to the flux surface ψ at time t is $\mathcal{E}_n(\psi, t)/t$. For sufficiently large t one finds

$$\langle\dot{\mathcal{E}}_n(\psi, t)\rangle \approx \frac{\pi}{4}c_n^2(\psi)\tilde{\Omega}_m^4 b_{m,0}^2\bar{\xi}_m^2(\psi, r_0)\delta(\tilde{\Omega}_m - \sigma_n), \tag{A4}$$

where $\delta(\tilde{\Omega}_m - \sigma_n)$ is a Dirac delta function. This expression is exact in the limit of $t \to \infty$. The total rate of energy transfer $\dot{E}$ from the crust to the Alfvén continuum is then obtained simply by integrating equation (A4) over ψ and summing over all n:

$$\begin{aligned}\dot{E} &= \sum_n \int_{\psi_{\min}}^{\psi_{\max}} \langle\dot{\mathcal{E}}_n(\psi)\rangle \mathrm{d}\psi \\ &= \sum_{n,k} \frac{\pi}{4}c_n^2(\psi_k)\tilde{\Omega}_m^4 b_{m,0}^2\bar{\xi}_m^2(\psi_k, r_0)\left.\frac{\mathrm{d}\psi}{\mathrm{d}\sigma_n}\right|_{\psi=\psi_k},\end{aligned} \tag{A5}$$

where ψ_k denotes flux surfaces that are in resonance with the crustal motion,$\sigma_n(\psi_k) = \tilde{\Omega}_m$. Since for a given n, the crustal mode may be in resonance with Alfvén modes in several flux surfaces ψ_k, the total energy transfer is obtained by summing over the index k. Equation (A5), which is the analogue of Fermi's golden rule in quantum physics, leads to a simple expression for the energy-damping time-scale $\tau_{E,m}$ ($=1/2\tau_{\mathrm{d},m}$) of the crustal mode:

$$\tau_{E,m} \sim \frac{E(t=0)}{\dot{E}} = \left[\sum_{n,k}\frac{\pi}{2}\tilde{\Omega}_m^2 c_n^2(\psi_k)\bar{\xi}_m^2\left.\frac{\mathrm{d}\psi}{\mathrm{d}\sigma_n}\right|_{\psi=\psi_k}\right]^{-1}, \tag{A6}$$

where $E(t=0) = 1/2\tilde{\Omega}_m^2 b_{m,0}^2$ is the initial energy of the mth crustal mode. Using numerical simulations, we verified the correctness of equation (A6). Even for very short damping times, that is, $\tau_{\mathrm{d}} = 2\tau_E \sim 2\pi/\tilde{\Omega}_m$, equation (A6) proves remarkably accurate.

This paper has been typeset from a TEX/LATEX file prepared by the author.